Pergamon

Int. J. Impact Engng Vol. 18, No. 3, pp. 247–264, 1996

0734–743X(95)00028-3
0734–743X/96 $15.00 + 0.00

ON THE *L/D* EFFECT FOR LONG-ROD PENETRATORS

CHARLES E. ANDERSON, Jr,† JAMES D. WALKER,†
STEPHAN J. BLESS‡ and YEHUDA PARTOM‡

†Southwest Research Institute, Materials and Structures Division, San Antonio, TX 78228, U.S.A.
and ‡Institute for Advanced Technology, The University of Texas at Austin, Austin, TX 78759, U.S.A.

(*Received* 18 *July* 1994; *in revised form* 28 *March* 1995)

Summary—A common measure of penetration efficiency is given by the depth of penetration P into a semi-infinite target normalized by the original length of the projectile L. It has been known for over 30 years that P/L depends upon the aspect ratio L/D for projectiles with relatively small aspect ratios, e.g. $1 \leqslant L/D \leqslant 10$. This influence of L/D on penetration is referred to as the *L/D effect*. Although observed, the L/D effect for large aspect ratio rods is not as well documented. Further, published penetration equations have not included the L/D effect for high aspect ratio rods. We have compiled a large quantity of experimental data that permits the quantification of the L/D effect for projectiles with aspect ratios of $10 \leqslant L/D \leqslant 30$. Numerical simulations reproduce the observed experimental behavior; thus, no new physics is required to explain the phenomenon. The numerical simulations allow investigation of the fundamental mechanics leading to a decrease in penetration efficiency with increasing aspect ratio.

NOTATION

d	plate thickness
D	projectile diameter
l	instantaneous projectile length
l_e	instantaneous eroded projectile length ($l_e \equiv L_0 - l$)
$\dot{l}$	projectile erosion rate
L, L_0	initial projectile length
L_r	residual projectile length
p	instantaneous depth of penetration
P	final depth of penetration
r^2	regression coefficient of determination
R_c	crater radius
R_m	target tensile strength
R_t	target resistance
s	extent of plastic zone in projectile
$T[V, \rho_p, \rho_t, Y_t, Y_p]$	hydrodynamic penetration theory
u	penetration velocity
v	projectile tail velocity
V	impact velocity
V_0	1.0 km/s
$\tilde{V}$	V/V_0
Y_p	projectile flow stress
Y_t	target flow stress
α	normalized (by the crater radius) extent of plastic flow in the target
θ	target obliquity
μ	proportionality constant
ρ_p	projectile density
ρ_t	target density
$\bar{\sigma}$	root mean standard error

INTRODUCTION

It is well known that penetration efficiency, as measured by the depth of penetration into a semi-infinite target normalized by the original length of the projectile (P/L), is greater for small L/D projectiles than for large L/D projectiles; for example, see Ref. [1]. The decrease in penetration efficiency with increasing aspect ratio is referred to as the *L/D effect*. Our interest here is the "long-rod" projectile, typically defined as $L/D \geqslant 10$. It was generally believed that the L/D effect saturated for $L/D > 10$, but Hohler and Stilp demonstrated in 1984 [2] that the

L/D effect continued to persist at aspect ratios of 32 (see also Ref. [3]). Although the L/D effect has been observed, it has not been explicitly discussed in the literature until recently [4, 5]. Rosenberg and Dekel [5] performed numerical simulations at an impact speed of 1.4 km/s and demonstrated that the L/D effect was predicted, and in agreement, with experimental data for L/D 10 and 20. They performed additional computations for L/D 30 and 40, and demonstrated that penetration efficiency continued to decrease with increasing aspect ratio; however, the authors do not provide an explanation for the cause of the effect.

Modified hydrodynamic theory, such as represented by the Tate model [6–8], does not predict an L/D effect, nor do other commonly used penetration formulae explicitly account for the L/D effect, e.g. Ref. [9]. Recently, Lanz and Odermatt [10] provided an empirical formula that explicitly includes a term to account for L/D. The expression is a curve fit to 41 data points for the ballistic limit plate thickness d as a function of impact velocity and target obliquity θ:

$$\frac{d}{L} = \left\{1 + \frac{3.77}{L/D}\left[1 - \tanh\left(\frac{L/D - 10}{6.89}\right)\right]\right\} \cdot \left(\frac{\rho_p}{\rho_t}\right)^{1/2} (\cos\theta)^{0.745} \cdot e^{-25.9 R_m/\rho_p V^2} \tag{1}$$

where R_m is the target tensile strength. In Eqn (1), the first term (within the curly brackets) becomes essentially 1 for $L/D \geqslant 20$, which means that for $L/D \geqslant 20$ the penetrable plate thickness is directly proportional to the penetrator length, and no longer is a function of L/D. It will be demonstrated below that the L/D effect continues to persist for $L/D \geqslant 20$.

An approach taken by other modelers is to use the modified hydrodynamic theory for all but the last diameter of the rod (for example, see Refs [3, 11–13]). The contribution to penetration for the last diameter of the rod is calculated from data for projectiles with an aspect ratio of 1. This last term accounts for residual crater growth, particularly at high velocities. Thus, the total depth of penetration can be written as some function of velocity times the length of the projectile (specifically, $L - D$) plus a term that is proportional to the diameter. At very high velocities, the penetration of a $L/D = 1$ projectile is proportional to the velocity to the two-thirds power [1, 12–14]. Written symbolically, this is:

$$P = T[V, \rho_p, \rho_t, Y_t, Y_p] \cdot (L - D) + \mu V^{2/3} D, \tag{2}$$

where $T[V, \rho_p, \rho_t, Y_t, Y_p]$ is the normalized depth of penetration from the modified hydrodynamic penetration model (this normalized depth is a function of the impact velocity and the densities and flow stresses of the projectile and target) and μ is a proportionality constant. Normalizing the above equation by the length of the projectile gives:

$$\frac{P}{L} = T[V, \rho_p, \rho_t, Y_t, Y_p] \cdot \left(1 - \frac{1}{L/D}\right) + \mu \frac{V^{2/3}}{L/D}. \tag{3}$$

As the L/D becomes large, two of the terms become negligible, i.e. P/L becomes independent of L/D. We can estimate the change in P/L for a change in L/D by taking the derivative of P/L with respect to L/D.

$$\frac{d(P/L)}{d(L/D)} = \frac{T[V, \rho_p, \rho_t, Y_t, Y_p]}{(L/D)^2} - \mu \frac{V^{2/3}}{(L/D)^2}. \tag{4}$$

Equation (4) can be used to make an estimate of the L/D effect, holding the velocity and materials constant. T is of the order of 1.0 [15] and $\mu V^{2/3}$ is of the order of 1.3 [1] for tungsten projectiles penetrating steel at an impact velocity of 1.5 km/s. Therefore, in going from a projectile with a L/D of 10 to 20, P/L will decrease by approximately 1.5%. As we shall see, this conclusion resulting from Eqns (3) and (4) underestimates the experimental (and numerical) L/D effect by a factor of 10.

The velocity range of interest for long-rod projectiles has traditionally been the so-called ordnance velocity range of 1.0–1.8 km/s. The remainder of this paper will focus on the L/D effect for long-rod projectiles in this velocity range. The L/D effect at higher velocities is examined in Ref. [16]. (At higher velocities, the L/D effect is given by Eqn (3).)

EXPERIMENTAL OBSERVATIONS

Part of the reason for the traditional viewpoint that the L/D effect saturates for large L/D ratios is the perceived scatter in experimental data. Care must be exercised in making comparisons. Penetration theories (for example, see [17]) predict that the depth of penetration is a strong function of target strength, and a much weaker function of projectile strength, and this is substantiated by experimental data [3, 18]. Specifically, we will focus on tungsten alloy projectiles and rolled homogeneous armor (RHA) targets (or RHA-like targets, e.g. 4340 steel targets hardened to approximately BHN 270). Our analysis of the experimental data has shown that the effect on penetration due to differences in density (tungsten content) are within the experimental scatter, but differences in target hardness and/or projectile flow characteristics (projectile alloy) can mask the L/D effect. Nominal properties of the various tungsten alloys are provided in Table 1 [19]. Because of potential differences between target hardnesses, and the exact processing of the tungsten alloy, we have compared data from the same laboratory, where possible, to minimize potential variation. However, we have combined data from different laboratories when the data are fairly sparse. Figures 1–4 compare normalized penetration as a function of impact velocity for L/D's of 10 and 15 [20–22]; 10 and 20 [20, 23, 24]; and two plots of 10, 15, and 30 [23, 24], respectively, for seven different tungsten alloys. The dashed lines in each of the figures are linear least squares fits of P/L as a function of impact velocity, for $V \leqslant 1.8$ km/s. For comparison purposes, the differences in normalized penetration at 1.5 km/s are given in Table 2. Clearly, the L/D effect continues to be prominent as the aspect ratio increases from 10 to 30, as also demonstrated in Refs [4, 5].

THE L/D EFFECT

It is instructive to examine P/L as a function of L/D. As already mentioned, linear least squares fits of P/L vs the impact velocity V were performed on the various experimental data groups. These provide a convenient method to estimate normalized penetration for three impact velocities: 1.2, 1.5, and 1.8 km/s. The results, along with additional data from Tate *et al.* [25], and the computational results to be discussed in the next section, are plotted in Fig. 5 as a function of L/D.

The first thing to note is that the numerical simulations predict the L/D effect for the larger L/D rods, and they are in good agreement with the experimental data. This is an important observation since this implies that no "new" physics must be invoked to explain the L/D effect. The second feature to note is that the curvature of the P/L vs L/D curve increases for decreasing L/D, particularly for low L/D. This is consistent with penetration efficiency being a strong function of aspect ratio for low L/D ratios. A third feature is that the curves appear to translate upward in P/L with increasing impact velocity without much change in shape. Although P/L is a strong function of impact velocity, this last observation implies that the L/D effect, at least in the ordnance velocity range, is either independent, or only a weak function, of impact velocity.

Table 1. Summary of nominal projectile characteristics [19]

Nomenclature	*Alloy materials*	*W content (% by weight)*	*Density (g/cm^3)*	*Strength (MPa)*
X30	W–Ni–Fe	90		
X27	W–Ni–Fe	91	17.34	895
X27C	W–Ni–Fe–Co	91	17.38	970
X27X	W–Ni–Co	91	17.45	1030
X21	W–Ni–Fe	93	17.74	920
X21C	W–Ni–Fe–Co	93	17.77	975
X9C	W–Ni–Fe–Co	97	18.61	985

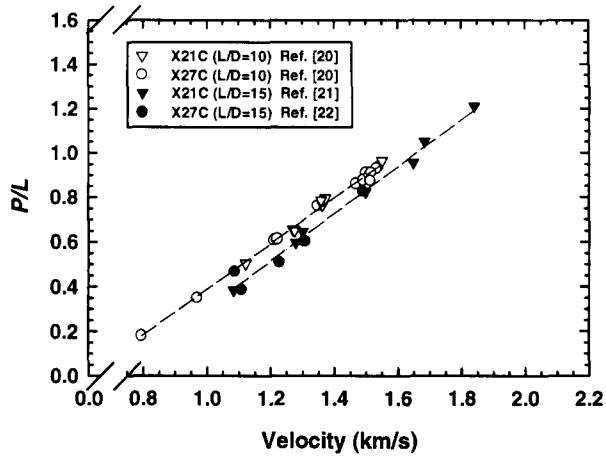

Fig. 1. *L/D* effect: *L/D* 10 and 15 projectiles (91%–93% W alloy, Ni–Fe–Co Matrix).

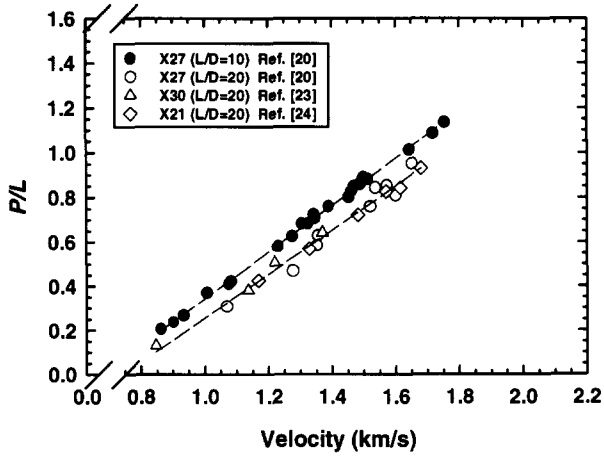

Fig. 2. *L/D* effect: *L/D* 10 and 20 projectiles (90–93% W alloy, Ni–Fe Matrix).

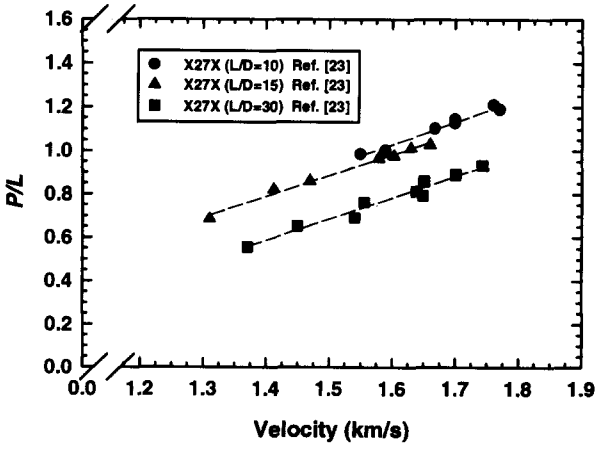

Fig. 3. *L/D* effect: *L/D* 10, 15 and 30 projectiles (91% W alloy, Ni–Co Matrix).

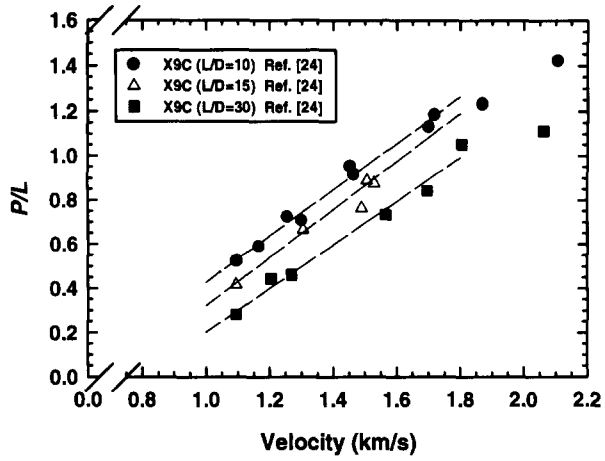

Fig. 4. L/D effect: L/D 10, 15 and 30 projectiles (97% W alloy, Ni–Fe–Co Matrix).

Table 2. Changes in penetration efficiency (%) at 1.5 km/s

Change in L/D	%	*Fig. No.*
L/D 10→15	−8	1
L/D 10→20	−14	2
L/D 10→15	−9	3
L/D 15→30	−22	3
L/D 10→30	−31	3
L/D 10→15	−4	4
L/D 15→30	−22	4
L/D 10→30	−26	4

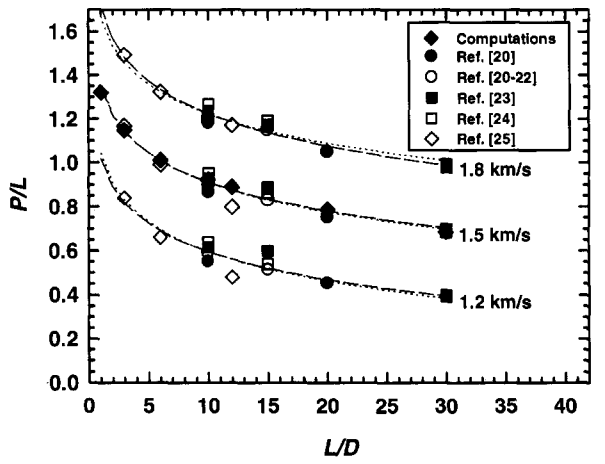

Fig. 5. Normalized penetration vs aspect ratio.

The dashed lines through the data (and computational points at 1.5 km/s) in Fig. 5 represent least-squares regression fits of the form $P/L = a + b\ln(L/D)$ that capture the overall decay of P/L with L/D. The regression parameters, root mean square error, and the coefficient of determination for the three impact velocities are given in Table 3. We have already observed that P/L vs L/D is relatively independent of impact velocity, and this is reflected in the regression parameter b being approximately equal for the three curves; and in fact, the differences in the three values for b are not statistically significant. Since P/L is essentially linear in the velocity range of 0.8–1.8 km/s, we can perform a regression fit to

Table 3. Regression coefficients for $P/L = a + b\ln(L/D)$

Velocity (*km/s*)	a (−)	b (−)	$\bar{\sigma}$ (−)	r^2 (−)
1.2	1.02	−0.184	0.041	0.892
1.5	1.34	−0.190	0.031	0.967
1.8	1.72	−0.214	0.029	0.959

$P/L = a + bV + c\ln(L/D)$ to obtain the constants a, b and c:

$$\frac{P}{L} = -0.209 + 1.044\tilde{V} - 0.194\ln\left(\frac{L}{D}\right), \tag{5}$$

where $\tilde{V} = V/V_0$, and V_0 is 1.0 km/s. The dotted lines in Fig. 5 were calculated from Eqn (5); the root mean square error between the data and Eqn (5) is 0.033, with an $r^2 = 0.986$. Equation (5) can be used to estimate the change in P/L as a function of L/D for tungsten-alloy projectiles into RHA steel:

$$\frac{\mathrm{d}(P/L)}{\mathrm{d}(L/D)} = -\frac{0.194}{L/D}. \tag{6}$$

Since Eqn (6) is based on the experimental data, it gives the correct dependence of P/L on L/D, e.g. at an impact velocity of 1.5 km/s, P/L will decrease by approximately 13% as the projectile L/D varies from 10 to 20.†

The change in P/L due to changing L/D from Tate-like theory, Eqn (4), is small because the L/D term in the denominator is squared. Thus, for a L/D 10 rod, $\mathrm{d}(P/L)/\mathrm{d}(L/D)$ is of the order of 1/100. However, for the experimental curve fit Eqn (5), the L/D term in the denominator is to the first power. Thus, $\mathrm{d}(P/L)/\mathrm{d}(L/D)$ is of the order of 1/10 for an L/D 10 rod. This observation leads to a significant conclusion. The first-order dependence implies that the L/D effect is not solely an "end" effect; i.e. it is not simply the result of the highly transient initial and terminal phases of impact. These transient phases are functions of the diameter of the projectile, and it was demonstrated in Eqns (2–4) that $\mathrm{d}(P/L)/\mathrm{d}(L/D)$ is proportional to $1/(L/D)^2$ for terms that depend linearly on D. Therefore, most of the L/D effect is due to how penetration occurs in the quasi-steady portion of penetration. After a presentation of the numerical results, it will be shown that the L/D effect is the result of the gradual decay in interface velocity during the quasi-steady-state phase of penetration.

NUMERICAL SIMULATIONS

The nonlinear, large deformation Eulerian wavecode CTH [26] was used to investigate penetration by projectiles of varying aspect ratios. The 2-D cylindrically symmetric option of CTH was used to simulate the projectile–target interaction. CTH uses a van Leer algorithm for second-order accurate advection that has been generalized to account for a non-uniform and finite grid, and multiple materials; CTH has an advanced material interface algorithm for the treatment of mixed cells. CTH allows the flow stress to be functions of strain, strain rate, and temperature [27, 28]. The Johnson–Cook model [29] with parameters for 4340 steel and a tungsten alloy was used for the computations. Table 4 lists the parameters used for this study. Seven zones were used to resolve the projectile radius; the zoning was square in the interaction region.

Two different sets of aspect ratios were computed: $L/D = 3$, 6 and 12, and $L/D = 10$, 20, and 30 projectiles. The two sets were run twice, once with constant diameter ($D = 0.30$ cm)

†Equation (1) does not reflect the change in penetration with L/D as seen in the experimental data: the d/L curve is too steep for $L/D < 10$, and it is too flat for $L/D > 15$.

Table 4. Constitutive parameters

	Y_0 (GPa)	B (GPa)	n (−)	C (−)	m (−)	T_{melt} (°K)	G (GPa)	ν (−)	Frac. stress (GPa)
Tungsten	1.51	0.177	0.12	0.016	1.00	1752	119	0.30	2.0
4340 Steel	1.189	0.765	0.26	0.014	1.03	1793	77.6	0.29	2.0

$$\sigma_{eq} = (Y_0 + B\varepsilon_p^n)\,[1 + C\ln(\dot{\varepsilon}_p/\dot{\varepsilon}_0)]\,(1 - \theta^{*m}) \quad \dot{\varepsilon}_0 = 1.0\,s^{-1} \quad \theta^* = \left(\frac{\theta - \theta_0}{\theta_m - \theta_0}\right) \quad \theta_0 = 298\,°K$$

Table 5. P/L from numerical simulations ($V_{impact} = 1.5$ km/s)

L/D	P/L constant D	P/L constant L
3	1.139	1.157
6	1.010	1.009
12	0.893	0.887
10	0.923	0.923
20	0.790	0.781
30	0.690	0.680

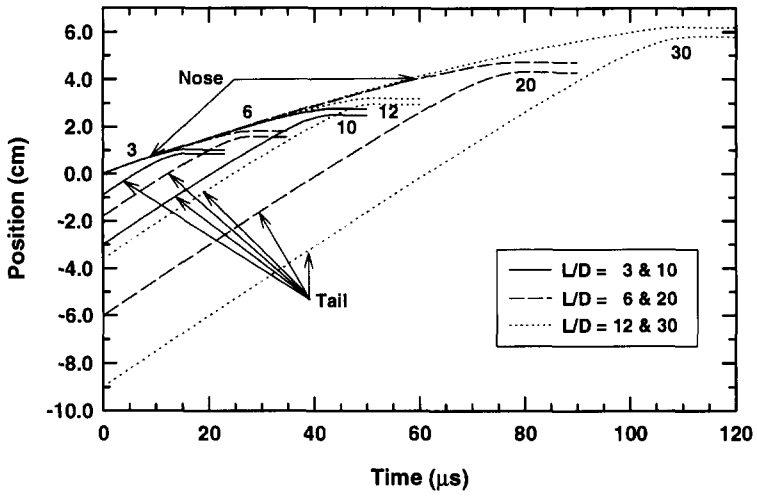

Fig. 6. Penetration (nose) and tail positions vs time for constant diameter projectiles.

projectiles, and the other with constant length ($L = 3.0$ cm) projectiles. The length or diameter of the projectiles was varied accordingly to give the proper aspect ratio. An impact velocity of 1.5 km/s was used for all the computations. The normalized penetrations as a function of L/D are summarized in Table 5.

Constant diameter projectiles

We focus first on constant diameter projectiles, so the length is the geometric dimension that changes to give different projectile aspect ratios. The positions of the nose and tail are plotted vs time in Fig. 6 for constant diameter projectiles. The nose (penetration) and tail velocities vs time for these projectiles are shown in Fig. 7. The nose and tail velocities are plotted as a function of the penetration depth in Fig. 8 for the various L/D's.

There are a number of important observations. The early time behavior of the projectiles is identical. As will be seen in the next section, the early time behavior is different if the diameters are different; therefore, the early time behavior scales with the diameter D.

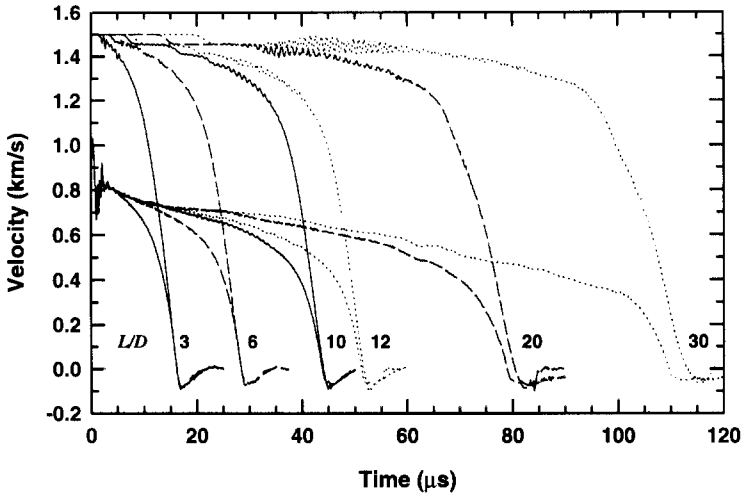

Fig. 7. Penetration (nose) and tail velocities vs time for constant diameter projectiles.

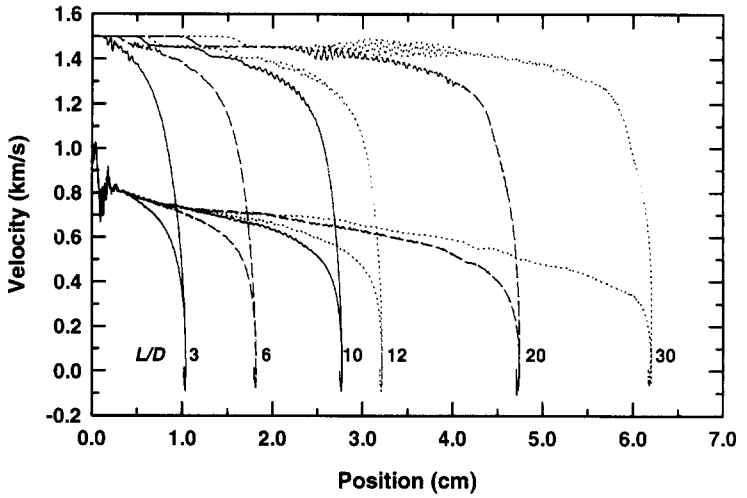

Fig. 8. Penetration (nose) and tail velocities vs penetration depth for constant diameter projectiles.

The step decrease in the tail velocity is caused by the arrival of the elastic wave—this disturbance was initiated at impact—travelling the length of the projectile. The elastic wave reflects off the free surface of the projectile, and travels back to the projectile–target interface. The penetration curves begin to deviate from one another when the elastic wave returns to the interface. This is the first length effect on penetration velocity. This effect is easiest to observe for projectiles that differ by factors of two in length.

The most important observation regards the penetration velocity in the so-called quasi-steady phase of penetration where the penetration velocity decreases with time. At early times, the penetration velocity curves overlay each other, suggesting that the penetration velocity scales with D and not with L. Beginning with the return of the elastic wave from the rear of the projectile, there is an L dependence in the penetration velocity. The tail velocities do not overlay; thus, the deceleration of the tail of the projectile does not scale with D.

Lastly, the terminal phase of deceleration, defined to be when the tail velocity begins the large deceleration near the end of penetration, is approximately the same for constant diameter projectiles. The terminal phases are almost parallel to each other in Figs 7 and 8; the fact that the terminal phases are slightly different is attributed to differences in the penetration velocity when the projectile enters the terminal phase. Therefore, the terminal phase scales with D.

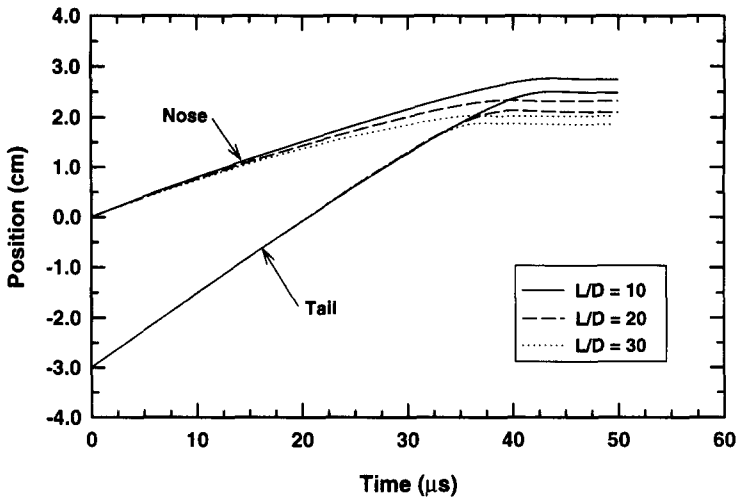

Fig. 9. Penetration (nose) and tail positions vs time for $L/D = 10, 20, 30$ (constant length) projectiles.

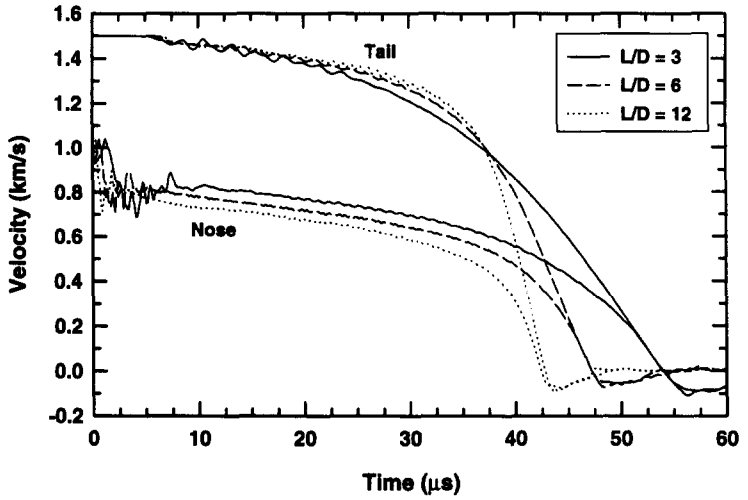

Fig. 10. Penetration (nose) and tail velocities vs time for $L/D = 3, 6, 12$ (constant length) projectiles.

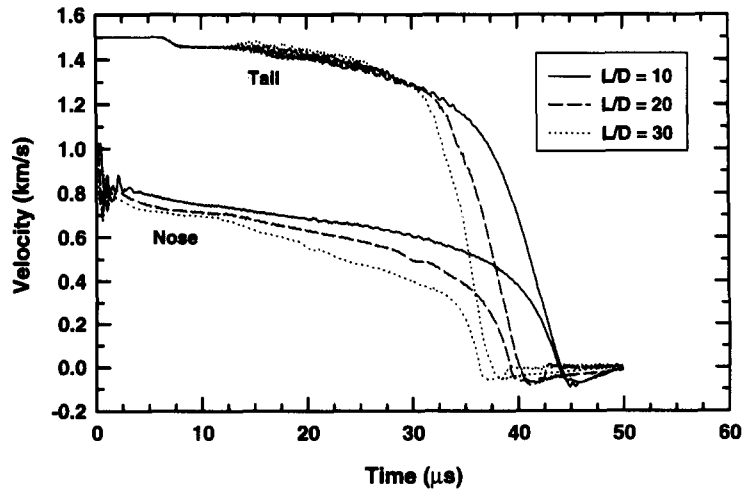

Fig. 11. Penetration (nose) and tail velocities vs time for $L/D = 10, 20, 30$ (constant length) projectiles.

Constant length projectiles

The positions of the nose and tail vs time are plotted for constant initial length projectiles with aspect ratios of 10, 20, and 30 in Fig. 9; the position–time curves for L/D 3, 6, and 12 look similar. The penetration and tail velocities vs time are plotted in Figs 10 and 11 for the two L/D groupings. Again, the impact velocity was 1.5 km/s for all the computations.

For constant length projectiles, the projectile emerges from the initial transient stage of penetration with different penetration velocities, Figs 10 and 11. This is a diameter effect; the smaller diameter projectiles take less time to transition to the quasi-steady-state penetration phase. Thus, at the same time in the penetration process, the penetration velocity is less than that of a larger diameter projectile, and similarly, the erosion rate is greater than that of a larger diameter projectile. This conclusion, drawn from the penetration and tail velocity histories, is confirmed in the position vs time plots of Fig. 9, which show that the larger L/D projectiles have less penetration than the shorter L/D projectiles for any specified time after impact.

The penetration velocity during quasi-steady penetration is less for smaller diameters, and suggests that the penetration velocity depends on D. Not only are they less, but Fig. 11 suggests that the slope decreases (becomes more negative) with decreasing diameter. This observation will be made quantitative in the Scaling and Penetration Efficiency section below. Since projectile tail velocities overlay for much of the penetration for the different diameters, it appears that the tail velocities scale with L. These two conclusions agree with those drawn from the constant diameter computer simulations.

From Figs 10 and 11, it is observed that the final deceleration phase of the projectiles is steeper for decreasing diameter (increasing aspect ratio). The deceleration phases were approximately parallel for constant diameter projectiles, thus, the deceleration phase scales with D. The steeper this deceleration, the more rapid the final phase of penetration and, ostensibly, the less penetration during this transient phase.

Residual length

The lengths of the residual projectile from the computations are plotted as a function of L/D in Fig. 12. Eulerian wavecodes do not model well the transition from eroding to rigid-body penetration [30], and L_r/D is different for the constant length and constant diameter computer runs. This scatter represents the uncertainty in mixed cell treatment. However, the overall trend seen in Fig. 12 should be correct. Included in the figure is a quadratic curve fit to these values, given by

$$L_r/D = 0.433 + 0.0533(L/D) - 7.243 \times 10^{-4}(L/D)^2. \tag{7}$$

Previous work [31] has shown that the length of the residual rod decreases with increasing

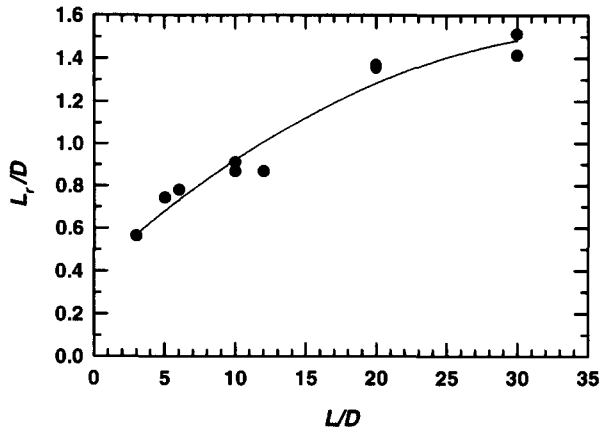

Fig. 12. Normalized residual projectile length vs L/D.

impact velocity. It is seen here that the residual rod length, in terms of the projectile diameter, increases with L/D.

Scaling and penetration efficiency

Comparing the P/L results in Table 5 at the same L/D (constant diameter and constant length computer runs), it is observed that the results are identical to within 1.5%. It was anticipated that P/L would depend only on the aspect ratio (for specified materials and impact velocity), and be independent of actual projectile dimensions (except for strain-rate effects which have been shown to be small over a scale factor of 10 [32]). But this is an important observation since it implies that the results of constant length projectiles can be scaled to constant diameter projectiles by multiplying the time and penetration depth by the geometric increase in length. When this is done, the results essentially overlay those of constant diameter. The significance of this observation is that conclusions can be made concerning the penetration response as a function of L/D and not L and D separately.

Examining the penetration histories of either Fig. 7, or Figs 10 and 11, we observe that the average penetration velocity in the quasi-steady penetration phase for the higher aspect ratio projectiles is less than the average penetration velocity of the shorter aspect ratio projectiles. Figures 13–15 quantitatively demonstrate how the efficiency of penetration decreases with

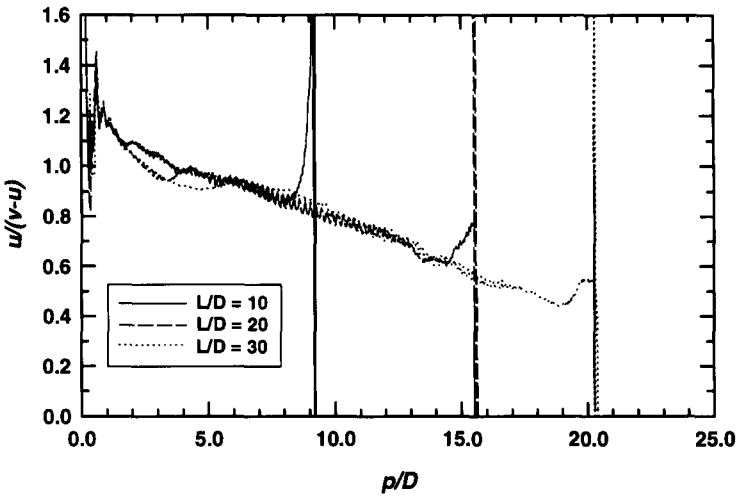

Fig. 13. Ratio of penetration velocity to erosion rate vs penetration in projectile diameters.

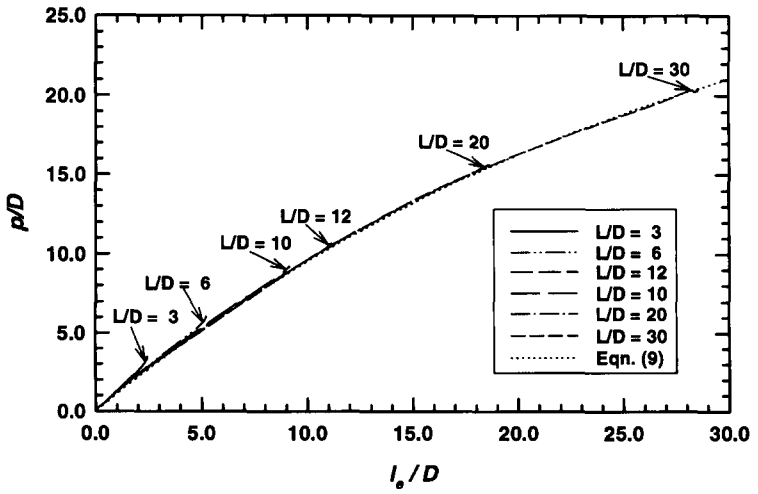

Fig. 14. Penetration in projectile diameters vs normalized projectile length eroded.

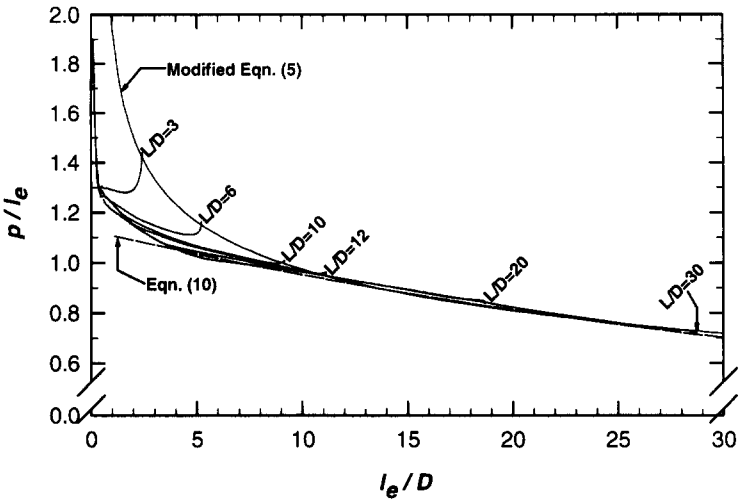

Fig. 15. Penetration per unit length rod eroded vs eroded rod measured in projectile diameters.

increasing length due to the deceleration of the projectile nose. One measure of the efficiency of eroding penetration, defined as the penetration velocity divided by the erosion rate,

$$\text{efficiency} = \frac{\text{penetration rate}}{\text{erosion rate}} = -\frac{\mathrm{d}p}{\mathrm{d}l} = \frac{u}{v-u},$$

where the lower case p denotes the instantaneous depth of penetration, is plotted in Fig. 13 as a function of penetration depth normalized by the projectile diameter. (This efficiency, $-\mathrm{d}p/\mathrm{d}l$, is an analog to the final depth of penetration P/L for eroding penetration where the projectile nearly completely erodes.) Although all the computational results were examined, only the results for L/D 10, 20, and 30 are presented for purposes of clarity. The vertical lines at approximately 9, 15.5, and 20.5 diameters of penetration represent where the projectile has gone rigid (and thus $v = u$) for the L/D 10, 20 and 30 projectiles, respectively. The curves from the three cases are seen to overlay each other. This is an important observation: the penetration efficiency is a function of the diameters of penetration, and this efficiency decreases as the projectile penetrates deeper into the target.

From Fig. 13, the ratio of penetration velocity to erosion rate is observed to decrease approximately linearly with respect to projectile penetration:

$$\frac{u}{v-u} \approx a - b\frac{p}{D}, \tag{8}$$

where the constants a and b are a function of the impact velocity. Noting that $\dot{p} = u$ and $(v-u) = -\dot{l}$, Eqn (8) can be integrated to give:

$$\frac{p}{D} = \frac{a}{b}(1 - \exp\{-b(L-l)/D\}), \tag{9}$$

where $l = L \equiv L_0$ at time $t = 0$. The quantity $L - l$ is the length of rod that has eroded, referred to as l_e. This gives penetration as a function of eroded projectile length. Assuming that the final length of the projectile is approximately zero, Eqn (9) gives the final depth of penetration as

$$\frac{P}{L} = a\frac{1-\exp\{-b(L/D)\}}{b(L/D)} = a\left\{1 - \frac{b}{2}\left(\frac{L}{D}\right) + \frac{b^2}{6}\left(\frac{L}{D}\right)^2 - \cdots\right\}. \tag{10}$$

Thus, the final depth of penetration shows an L/D dependence when the efficiency of penetration is dependent on the number of diameters of penetration. We note that Eqn (10) does not have the same form as the empirical curve fit to the data, Eqn (5). Using values for a and b (given below), Eqn (10) provides a reasonable estimate of the experimental data for

$L/D > 7$, but it certainly is not as accurate as Eqn (5), primarily because of the assumption that the residual rod length is zero.

An alternative way of examining the penetration efficiency is to examine the variables suggested by Eqn (9), namely p/D vs l_e/D, as in Fig. 14. l_e/D represents the amount of projectile eroded, in projectile diameters, to achieve p/D penetration. All six L/D computations are shown. The results for the different L/D projectiles are essentially identical where the curves overlap, although there is a small amount of deviation during the late phase of penetration for the short L/D's. The p/D curve is concave down, so that for increasing aspect ratio, P/L will decrease. Effectively, the results of Fig. 14 show that the penetration per length of eroded rod decreases as the projectile penetrates the target. Also shown on this plot is Eqn (9), where the coefficients $a = 1.127$ and $b = 0.03455$ were obtained by the linear fit of Eqn (8) to Fig. 13. The agreement is quite good, which demonstrates that examining the efficiency $u/(v-u)$ provides much information about total penetration of an eroding projectile.

A final figure in this series, Fig. 15, is similar to the previous one, but plotting p/l_e (instead of p/D) vs the length eroded l_e/D for all six L/D's. Also on this plot is Eqn (10), with the coefficients obtained above. This expression shows that the linear decrease in $u/(v-u)$ agrees with the quasi-steady penetration of the projectiles. For $L/D < 10$, the final state deviates from the assumption of a linear decrease of the penetration velocity with time (the quasi-steady-state penetration regime). This deviation is due to the final transient penetration phase where the computational curves become vertical when erosion ceases. However, by the time $L/D = 10$, the initial and final transients are negligible relative to total penetration, and the L/D effect is completely due to the quasi-steady portion of penetration. Even for $l_e/D < 10$ penetration, it is clear that there is a quasi-steady penetration phase during which all the projectiles have the same penetration vs eroded length. Therefore, the deviation of Eqn (10) from the computational results for small L/D demonstates that the final transients play a role in final penetration depth for $L/D < 10$, while the agreement for $L/D > 10$ shows that the decay in the penetration velocity during the quasi-steady phase is primarily responsible for the L/D effect for long rods in the ordnance velocity range.

Lastly, another analytical expression is plotted in Fig. 15. This expression is derived from Eqn (5). The penetration depth obtained from Eqn (5) is divided by the initial length (L) minus the residual length (L_r) obtained from Eqn (7), and this is plotted vs $(L-L_r)/D$. The agreement between this modified Eqn (5) and the computational results is quite remarkable. This verifies Eqn (5) and Eqn (7), and further confirms the role of transients for $L/D < 10$ penetration.

In summary, the penetration velocity during the quasi-steady phase of penetration decreases in a manner that is dependent on the diameter of the projectile; therefore, the time-weighted average penetration velocity decreases for increasing aspect ratio. Since penetration is a strong function of velocity in the ordnance velocity range for tungsten alloy projectiles into armor steel, the higher aspect ratio projectile does not penetrate as deeply when normalized by the original length of the projectile. The penetration in projectile diameters vs the projectile's eroded length in projectile diameters can be represented by a single curve, regardless of initial aspect ratio of the projectiles. This curve is concave down, showing a diminishing return in penetration depth per eroded projectile length.

A SIMPLE MODEL

To demonstrate that the origin of the effect is due to the decrease in the penetration velocity depending on the projectile diameter, a simple model of eroding penetration is discussed. First, there are two equations that are common to the various long-rod penetration models:

$$\dot{v} = -\frac{Y_p}{\rho_p l} \tag{11a}$$

$$\dot{l} = -(v-u). \tag{11b}$$

The first equation, Eqn (11a), approximates the deceleration of the back end of the projectile, where l is the instantaneous length of the projectile. The second equation, Eqn (11b), simply states that the erosion rate of the projectile is the difference in the tail velocity v and the penetration velocity u. To complete the model, a third equation is required to determine the interface velocity u. The initial conditions are the impact velocity and the initial projectile length L. These equations hold until either $v = u$ (the projectile no longer erodes) or $u = 0$ (penetration has ceased).

If the equation for u does not depend on D, then there will be no L/D effect because D nowhere enters into the equations. For example, the Tate model [6, 7] does not predict an L/D effect; the u from the Tate model is obtained from:

$$\tfrac{1}{2}\rho_p(v-u)^2 + Y_p = \tfrac{1}{2}\rho_t u^2 + R_t, \tag{12}$$

where R_t is the target resistance to penetration [6–8]. This can be written in rate form as

$$\dot{u} = \frac{\rho_p(v-u)}{\rho_t u + \rho_p(v-u)}\dot{v} = -\frac{(v-u)}{\rho_t u + \rho_p(v-u)}\frac{Y_p}{l}. \tag{13}$$

There is no explicit D dependence, and so the model has no L/D dependence. Deceleration of the projectile comes from Eqns (11a) and (13), with the result that the average penetration velocity for different aspect ratios are the same in the Tate model.

As a second example, consider Eqn (8), the linear fit of the penetration efficiency in terms of the penetration depth (Fig. 13). Using $\dot{p} = u$, this equation provides the following equation for $\dot{u}$:

$$\dot{u} = \frac{u}{v}\left(\dot{v} - (v-u)^2\frac{b}{D}\right) = -\frac{u}{v}\left(\frac{Y_p}{\rho_p l} + (v-u)^2\frac{b}{D}\right). \tag{14}$$

Since the deceleration of the penetration velocity u depends explicitly on D, there will be an L/D effect. To demonstrate the dependence of the L/D effect on the term containing b, Fig. 16 plots four cases: $b = 0$, $b = 0.02$, $b = 0.03455$ (the fit from Fig. 13), and $b = 0.05$. In all cases, $a = 1.127$ (the fit from Fig. 13) provided an initial $u = 0.79$ km/s from Eqn (8), for the initial $v = 1.5$ km/s. The densities of the projectile and the target were 17.3 g/cm^3 and 7.85 g/cm^3, respectively. It is seen that when $b = 0$ there is no L/D effect since D drops out of the $\dot{u}$ equation. However, for increasing b, the L/D effect becomes more prominent. Also plotted in Fig. 16 is the P/L curve of Eqn (5). It is seen that the penetration depth from the simple model does not quite match the curve fit to experimental data, Eqn (5). The problem, for large

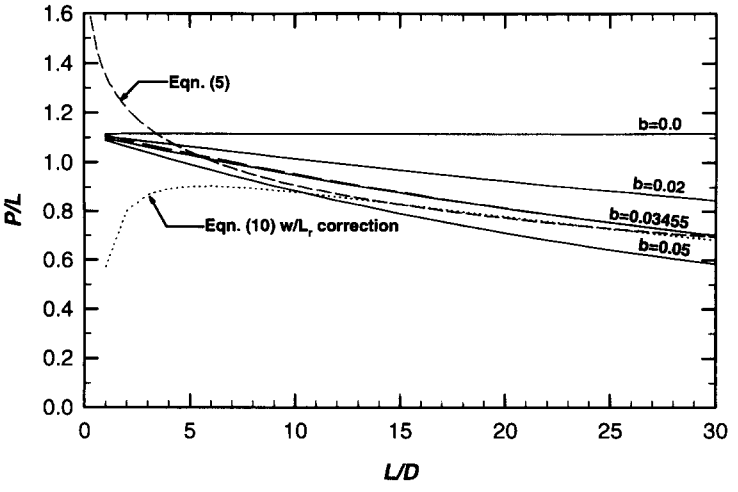

Fig. 16. Penetration of the simple model.

L/D, lies in the stopping criteria for the model described by Eqns (11) and (14). In this simple model, the rod nearly completely erodes and the $v = u$ criterion terminates penetration. The residual length of the projectile is much smaller than that seen in the computations. If instead the stopping criterion for the model is defined so that penetration ceases when l equals the residual rod length of Eqn (7), then the dotted curve in the graph results. Though it does not do well for low L/D where the final transient phase is important, the experimental curve and the model curve overlay for higher L/D, demonstrating that Eqn (8) is a good representation of the behavior of the penetration velocity for large aspect ratio rods.

As a particular corollary to the observation that $\dot{u}$ must explicitly depend on D, we can conclude that if $\dot{u} \equiv 0$ then there will be no L/D effect. Thus, if penetration were truly steady state, there would be no L/D effect, since u would remain constant, and $\dot{u}$, being zero, would not depend on D. The L/D effect is due to the decrease (in general, the change) in penetration velocity during penetration. The decrease (change) in penetration velocity depends on a length scale that is proportional to the diameter of the projectile.

Since we have demonstrated that the L/D effect requires a nonzero $\dot{u}$, it is desirable to know why the penetration velocity decays on physical grounds. In a recent penetration model by Walker and Anderson [33], the axial momentum equation is integrated along the centerline of penetration. The transient terms have been retained,† and the resulting expression contains a deceleration term, $\dot{u}$, for the penetration velocity:

$$\rho_p \dot{v}(l-s) + \dot{u}\left\{\rho_p s + \rho_t R_c \frac{\alpha - 1}{\alpha + 1}\right\} + \rho_p \left(\frac{v \dot{-} u}{s}\right)\frac{s^2}{2} + \rho_t \dot{\alpha} \frac{2R_c u}{(\alpha+1)^2}$$
$$= \tfrac{1}{2}\rho_p (v-u)^2 - \{\tfrac{1}{2}\rho_t u^2 + \tfrac{7}{3}\ln(\alpha) Y_t\}. \tag{15}$$

In Eqn (15), s is the extent of the plastic zone in the projectile, and α represents the extent of plastic flow in the target in terms of the crater radius R_c. The deceleration of the tail of the projectile is essentially given by Eqn (11a), but with l replaced by $(l - s)$; the time rate of change of the length of the projectile is given by Eqn (11b). Both R_c and s scale with the projectile radius, and both multiply $\dot{u}$. Therefore, the transient terms, which originate from the inertia of the velocity field in the target and change in the extents of the plastic zone in the target and in the projectile, introduce a D dependence in $\dot{u}$.‡ However, as will be discussed below, the L/D effect is mostly due to a D dependence in α.

It turns out that Eqn (15), with α calculated by a cavity expansion method [33], does not produce as great an L/D effect as is seen in experiments. Although the p/D vs l_e/D curves are concave down as in the numerical simulations, the curvatures are not as great, and the curves do not overlay for the various L/D's as they do for the numerical simulations. These effects combine to give a $\mathrm{d}(P/L)/\mathrm{d}(L/D)$ of approximately one-fourth that seen in the simulations and the experiments (closer to an $(L/D)^2$ dependency than an L/D dependency). The model can be used to explore what is necessary to give the appropriate L/D dependence. It is found that the extent of the plastic zone within the target must increase as a function of penetration depth in terms of projectile diameters during quasi-steady penetration. In contrast, in the current model formulation, the α calculated with a cavity expansion expression is relatively constant with time during the quasi-steady-state portion of penetration (α does increase a small amount since it depends on the penetration velocity). An α that increases during penetration was anticipated by comparing the model against penetration velocity [35]. Also, the computational results of Ref. [17] indicated that the overall target resistance increases with time during quasi-steady penetration, suggesting that α should also increase, thereby supporting this conclusion. By taking $R_t = \frac{7}{3}\ln(\alpha) Y_t$ in the Tate model, with α dependent on the depth of penetration in projectile diameters as above, a large L/D effect ensues in the Tate model. Thus, the large L/D effect is mostly due to the D dependent increase in α and does not

†Tate modified his original model and acceleration terms were not neglected [34]. The deceleration term depends on the crater radius, and hence D. However, the implications of including such terms were not explored.

‡We note that if $R_c \to 0$ and $s \to 0$ in Eqn (15), then no L/D effect would be expected. When this limit is taken, Eqn (15) reduces to Eqn (12), with $R_t = \frac{7}{3}\ln(\alpha) Y_t$. This is simply the original Tate model which has no L/D effect.

arise solely through the transient terms in Eqn (15). Clearly, as stated in Ref. [33], the determination of the extent of the plastic zone in the target is an area requiring further research.

Computer simulations were performed where the projectile strength was set to zero (at an impact velocity of 1.5 km/s). Normalized penetrations for these fluid projectiles were 0.75, 0.75, and 0.72 for the L/D 10, 20, and 30 projectiles, respectively. However, the mechanics of penetration changes dramatically during the terminal stage of penetration for the L/D 20 and 30 projectiles. There appears to be some sort of focusing effect of the projectile material towards the centerline, through an interaction of projectile material with the crater walls, that results in a very narrow crater and enhanced penetration. If, instead, an estimate of penetration is made by extrapolating the normal penetration behavior, then normalized penetrations are estimated to be 0.75, 0.67, and 0.56, respectively, for the L/D 10, 20, and 30 projectiles. Although these points lay below the 1.5-km/s curve in Fig. 5, the overall trend is similar to the curve for which the projectile has strength. Thus, it is concluded that the L/D effect cannot be attributed to strength effects of the projectile.

However, penetration performance can be modified by failure mechanisms at the nose of the projectile. In the work here, the failure model consisted of the insertion of void into computational cells when the material stress exceeded a tensile criterion; thus, all computations assumed the same operative dynamics. Magness has demonstrated that the improved performance of DU–0.75% Ti projectiles as compared to tungsten alloy projectiles is due to the propensity of the DU–0.75% Ti alloy to form adiabatic shear bands during penetration [24]. Calculations by Parton and Yaziv [4] and Partom [36] show that penetration efficiency can be modified by changing the plastic flow response of the projectile material. This influence has been determined through changes of a strain-to-failure criterion for penetrator material [4] and through manipulation of the constitutive response of the projectile material [36]. These results demonstrate that the dynamic flow behavior of the projectile plays a role in the overall penetration process, but the results here suggest that the origins of the L/D effect lay in the behavior of the target.

SUMMARY

The degraded performance of penetration, as measured by a decrease in normalized penetration P/L, as the aspect ratio L/D of the projectile increases has been examined. The traditional hydrodynamic-plus-strength theories of penetration do not predict an L/D effect, and greatly underpredict the effect when modified to account for residual crater growth at the end of penetration. Experimental data from a variety of sources (tungsten alloy projectiles into RHA) were used to quantify the L/D effect. In the ordnance velocity range of $0.8 \leqslant V \leqslant 1.8$ km/s, it was shown (empirically) to a very good approximation that penetration performance degrades as $\ln(L/D)$ for $1 \leqslant L/D \leqslant 30$.

Numerical simulations were performed, and the calculated P/L's were in good agreement with experimental data as a function of L/D. The computational results scale between constant diameter projectiles and constant length projectiles; therefore, conclusions could be made concerning variations in L/D, independent of specific L's and D's. It was shown that the average penetration velocity decreases for an increase in projectile aspect ratio, and that this decrease in penetration velocity is the cause of the L/D effect for large aspect ratio projectiles. (It was also demonstrated that for small aspect ratio rods, transients at the end of penetration contribute significantly to the L/D effect.) The deceleration of the front end of the projectile depends on a length scale that is proportional to projectile diameter, whereas total penetration time is proportional to the projectile length; the combination of these two length scales leads to the L/D effect. Using analytical modeling, the origins of the L/D effect were explored. It was suggested that growth of the plastic zone within the target contributes to the L/D effect. If the penetration velocity were constant through the whole penetration process, there would be no L/D effect. For example, it is demonstrated in Ref. [16] that at higher impact velocities (above 2.0 km/s), where the penetration velocity is constant in the "steady-

state" region, the L/D effect results from the terminal (transient) phase of penetration and not from the quasi-steady phase. This is in contrast to lower velocity penetration.

Acknowledgements—This work was performed under Contract No. DAAL03-92-K-001, administered by the U.S. Army Research Office, and under Contract No. UT/SWRI-0009 with the Institute for Advanced Technology. The authors would like to thank Mr. Dick Sharron for his support with the computations.

REFERENCES

1. C. E. Anderson, Jr., D. L. Littlefield, N. W. Blaylock, S. J. Bless and R. Subramanian, The penetration performance of short L/D projectiles. In *High-Pressure Science and Technology—1993*, pp. 1809–1812 (Edited by S. C. Schmidt, J. W. Shaner, G. A. Smara and M. Ross). AIP, NY (1994).
2. V. Hohler and A. Stilp, Influence of the length-to-diameter ratio in the range from 1 to 32 on the penetration performance of rod projectiles. *Proc. 8th Int. Symp. on Ballistics*, pp. IB13-IB19. Orlando, FL, Oct. 23–25 (1984).
3. V. Hohler and A. Stilp, Hypervelocity impact of rod projectiles with L/D from 1 to 32. *Int. J. Impact Engng* **5**, 323–331 (1987).
4. Y. Partom and D. Yaziv, Penetration of $L/D = 10$ and 20 tungsten alloy projectiles into RHA. In *High-Pressure Science and Technology—1993*, pp. 1801–1804 (Edited by S. C. Schmidt, J. W. Shaner, G. A. Smara and M. Ross). AIP, NY (1994).
5. Z. Rosenberg and E. Dekel, The relation between the penetration capability of long rods and their length to diameter ratio. *Int. J. Impact Engng* **15**, 125–129 (1994).
6. A. Tate, A theory for the deceleration of long rods after impact. *J. Mech. Phys. Solids* **15**, 387–399 (1967).
7. A. Tate, Further results in the theory of long rod penetration. *J. Mech. Phys. Solids* **17**, 141–150 (1969).
8. A. Tate, Long rod penetration models—Part II. Extensions to the hydrodynamic theory of penetration. *Int. J. Mech. Sci.* **28**, 599–612 (1986).
9. B. R. Sorensen, K. D. Kimsey, G. F. Silsby, D. R. Scheffler, T. M. Sherrick and W. S. deRosset, High velocity penetration of steel targets. *Int. J. Impact Engng* **11**, 107–119 (1991).
10. W. Lanz and W. Odermatt, Penetration limits of conventional large caliber anti tank guns/kinetic energy projectile. *Proc. 13th Int. Symp. on Ballistics*, Vol. 3, pp. 225–233, Stockholm, Sweden, June 1–3 (1992).
11. D. R. Christman and J. W. Gehring, Analysis of high-velocity projectile penetration mechanics. *J. Appl. Phys.* **37**, 1579–1587 (1966).
12. W. Herrmann and J. S. Wilbeck, Review of hypervelocity penetration theories. *Int. J. Impact Engng* **5**, 307–322 (1987).
13. A. C. Charters, T. L. Menna and A. J. Piekutowski, Penetration dynamics of rods from direct ballistic tests of advanced armor components at 2–3 km/s. *Int. J. Impact Engng* **10**, 93–106 (1990).
14. D. L. Orphal, C. E. Anderson, Jr. and R. R. Franzen, Impact calculations of $L/D \leqslant 1$ penetrators. *Proc. 12th Int. Symp. on Ballistics*, Vol. 1, pp. 458–464 (1990).
15. C. E. Anderson, Jr. and J. D. Walker, An examination of long-rod penetration. *Int. J. Impact Engng* **11**, 481–501 (1991).
16. C. E. Anderson, Jr., J. D. Walker, S. J. Bless and T. R. Sharron, On the velocity dependence of the L/D effect for long-rod penetrators. *Int. J. Impact Engng* **17**, 13–24 (1995).
17. C. E. Anderson, Jr., J. D. Walker and G. E. Hauver, Target resistance for long-rod penetration into semi-infinite targets. *Nucl. Engng and Design* **138**, 93–104 (1992).
18. T. W. Bjerke, The effect of material strength on segment penetration behavior. ARL-MR-51, U.S. Army Research Laboratory, Aberdeen Proving Ground, MD (1993).
19. S. G. Caldwell, personal correspondence, Teledyne Firth Sterling, Ordnance Division, #1 Teledyne Place, Interchange City Industrial Park, Lavergne, TN (1988).
20. P. Woolsey, in "A Penetration Mechanics Database", by C. E. Anderson, Jr., B. L. Morris, and D. L. Littlefield, SwRI Report 3593/001, AD-A246351, Southwest Research Institute, San Antonio, TX (1992).
21. W. Leonard, L. Magness, Jr. and D. Kapoor, Ballistic evaluation of thermo-mechanically processed tungsten. BRL-TR-3326, USA Ballistic Research Laboratory, Aberdeen Proving Ground, MD (1992).
22. C. E. Anderson, Jr. and B. L. Morris, The ballistic performance of confined Al_2O_3 ceramic tiles. *Int. J. Impact Engng* **12**, 167–187 (1992).
23. C. E. Anderson, Jr., Unpublished data
24. L. S. Magness and T. G. Farrand, Deformation behavior and its relationship to the penetration performance of high-density KE penetrator materials. *Army Science Conf.*, Durham, NC (1990).
25. A. Tate, K. E. B. Green, P. C. Chamberlain and R. G. Baker, Model scale experiments on long rod penetration. *Proc. 4th Int. Symp. on Ballistics*, Naval Postgraduate School, Monterey, CA, October 17–19 (1978).
26. J. M. McGlaun, S. L. Thompson and M. G. Elrick, CTH: a three-dimensional shock wave physics code. *Int. J. Impact Engng* **10**, 351–360 (1990).
27. W. W. Predebon, C. E. Anderson, Jr. and J. D. Walker, Inclusion of evolutionary damage measures in Eulerian wavecodes. *Comput. Mech.* **7**, 221–236 (1991).
28. S. Silling, Stability and accuracy of differencing methods for viscoplastic models in wavecodes. *J. Comput. Phys.* **104**, 30–40 (1993).
29. G. R. Johnson and W. H. Cook, Fracture characteristics of three metals subjected to various strains, strain rates, temperatures, and pressures. *Engng Fracture Mech.* **21**, 31–48 (1985).
30. J. D. Walker and C. E. Anderson, Jr., Multi-material velocities for mixed cells. In *High-Pressure Science and Technology*—1993, pp. 1773–1776 (Edited by S. C. Schmidt, J. W. Shaner, G. A. Smara and M. Ross). AIP, NY (1994).

31. C. E. Anderson, Jr., D. L. Littlefield and J. D. Walker, Long-rod penetration, target resistance, and hypervelocity impact. *Int. J. Impact Engng* **14**, 1–12 (1993).
32. C. E. Anderson, Jr., S. A. Mullin and C. J. Kuhlman, Computer simulations of strain-rate effects in replica scale model penetration experiments. *Int. J. Impact Engng* **13**, 35–52 (1993).
33. J. D. Walker and C. E. Anderson, Jr., A time-dependent model for long-rod penetration. *Int. J. Impact Engng* **16**, 19–48 (1995).
34. A. Tate, Long rod penetration models—Part 1. A flow field model for high speed long rod penetration. *Int. J. Mech. Sci.* **28**, 535–548 (1986).
35. J. D. Walker and C. E. Anderson, Jr., A transient model for long-rod penetration. *13th Int. Symp. on Ballistics*, Stockholm, Sweden, June 1–3 (1992).
36. Y. Partom, Projectile-flow effect for long rod penetration. Report IAT.R.0036, Institute for Advanced Technology, The University of Texas, Austin, TX (1994).